



Nitrogen Doped Carbon Nanosheets Encapsulated *in situ* Generated Sulfur Enable High Capacity and Superior Rate Cathode for Li-S Batteries

Zhijun Guo¹, Xiaoyu Feng^{1*}, Xingxing Li¹, Xuming Zhang¹, Xiang Peng², Hao Song¹, Jijiang Fu¹, Kang Ding¹, Xian Huang¹ and Biao Gao^{1*}

¹ The State Key Laboratory of Refractories and Metallurgy and Institute of Advanced Materials and Nanotechnology, Wuhan University of Science and Technology, Wuhan, China, ² School of Materials Science and Engineering, Wuhan Institute of Technology, Wuhan, China

OPEN ACCESS

Edited by:

Qiaobao Zhang,
Xiamen University, China

Reviewed by:

Ruitao Lv,
Tsinghua University, China
Xiwen Wang,
Hunan University, China

*Correspondence:

Xiaoyu Feng
fengxiaoyu@wust.edu.cn
Biao Gao
gaobiao@wust.edu.cn

Specialty section:

This article was submitted to
Nanoscience,
a section of the journal
Frontiers in Chemistry

Received: 31 July 2018

Accepted: 30 August 2018

Published: 25 September 2018

Citation:

Guo Z, Feng X, Li X, Zhang X, Peng X, Song H, Fu J, Ding K, Huang X and Gao B (2018) Nitrogen Doped Carbon Nanosheets Encapsulated *in situ* Generated Sulfur Enable High Capacity and Superior Rate Cathode for Li-S Batteries. *Front. Chem.* 6:429. doi: 10.3389/fchem.2018.00429

Lithium-sulfur batteries (LSBs), with large specific capacity (1,675 mAh g⁻¹), are regarded as the most likely alternative to the traditional Lithium-ion batteries. However, the intrinsic insulation and dramatic volume change of sulfur, as well as serious shuttle effect of polysulfides hinder their practical implementation. Herein, we develop three-dimensional micron flowers assembled by nitrogen doped carbon (NC) nanosheets with sulfur encapsulated (S@NC-NSs) as a promising cathode for Li-S to overcome the forementioned obstacles. The *in situ* generated S layer adheres to the inner surface of the hollow and micro-porous NC shell with fruitful O/N containing groups endowing both efficient physical trapping and chemical anchoring of polysulfides. Meanwhile, such a novel carbon shell helps to bear dramatic volume change and provides a fast way for electron transfer during cycling. Consequently, the S@NC-NSs demonstrate a high capacity (1,238 mAh g⁻¹ at 0.2 C; 1.0 C = 1,675 mA g⁻¹), superior rate performance with a capacity retention of 57.8% when the current density increases 25 times from 0.2 to 5.0 C, as well as outstanding cycling performance with an ultralow capacity fading of only 0.064% after 200 cycles at a high current density of 5.0 C.

Keywords: *in situ* generated sulfur, nitrogen doped carbon, cathode, chemical anchoring, physical trapping, lithium-sulfur batteries

INTRODUCTION

Lithium-sulfur batteries (LSBs) own many advantages including high energy density (2,600 Wh kg⁻¹, five times larger than lithium ion batteries), natural abundance, and environmental friendliness (Rehman et al., 2016; Xu et al., 2017; Qu et al., 2018; Zhang et al., 2018). Thus, LSBs have become one of the most promising candidates for large-scale energy storage and long endurance electric vehicles applications (Seh et al., 2016; Chen et al., 2017; Ye et al., 2018). However, the practical implement of the LSBs is impeded by several challenges, such as electronically and ionically insulating of S, large volume change (~80%) during cycling, as well as shuttle effect induced by the high solubility and mobility of the lithium polysulfides (LiPSs) intermediates. To tackle with the above issues, one of the effective routes is encapsulating S into conductive

carbon hosts [active carbon (Moreno et al., 2015; Li F. et al., 2017), carbon spheres (Qu et al., 2013; Zhou et al., 2017), graphene (Tang et al., 2016; Du et al., 2017), carbon nanotubes (Li M. et al., 2017) and nanofibers (Liu et al., 2018)] with high porosity or/and high specific surface area to improve electron/ion conductivity, tolerate volumetric expansion and physically trap LiPSs. Nevertheless, the weak interaction between nonpolar carbon and polar LiPSs inevitably results in effusion and irreversible loss of LiPSs from the cathodes and thus rapid capacity fading during cycling. Polar metal oxides, metal sulfides, metal carbides, and metal nitrides have recently been explored as efficient host materials for S cathodes in LSBs and the S/metal oxide composites have been demonstrated to achieve improved cycle stability *via* chemical anchoring between the metal oxide and LiPSs in the cathodes. However, limited active sites of these polar hosts with low surface area lead to low immobilization efficiency for LiPSs (Shi et al., 2018). Recently, heteroatom doping (e.g., N, S, P) has been developed to enable carbon hosts to be polarity and retain the large surface area simultaneously, which can not only trap the LiPSs physically, but also improve conversion kinetics from LiPSs into solid Li_2S (Wang X et al., 2014; Pang et al., 2015; Zhou et al., 2015a; Wang et al., 2016, 2019; Li C. et al., 2018). Moreover, two-dimensional (2D) nanocarbon materials have drawn special attention as S hosts due to shorter ion/electron transport distance and more active sites (Chabu et al., 2017; Song et al., 2018; Sun et al., 2018; Wang Q et al., 2018).

In this work, we develop a hierarchical three-dimensional (3D) nano-flowers host consisting of hollow 2D nitrogen doped carbon nanosheets (NC-NSs) with micro-porosity shell as the S host. The S is encapsulated in the 2D NC-NSs (S@NC-NSs) with a thickness of 25–40 nm *via in-situ* oxidization of NC coated ZnS NSs (ZnS@NC-NSs) by Fe^{3+} . Such unique hierarchical S@NC-NSs assembled by nanosheets endow several advantages as the S host for Li-S: Firstly, the NC shell with typical micro-sized pores can not only physically confine the LiPSs but also chemically anchor LiPSs *via* rich N/O containing functional groups; Secondly, the *in situ* generated S is totally encapsulated in the NC shell, resulting high utilization; Thirdly, S@NC-NSs have large inner space and the elastic carbon shell can accommodate the volume expansion of the S during lithiation; Lastly, 3D hierarchical nano-flowers structure assembled by 2D NC-NSs provides a fast conductive network, and integral structure supporters. Ultimately, the S@NC-NSs deliver a high specific capacity of 1,238 mAh g^{-1} at a current density of 0.2 C (1.0 C = 1,675 mA g^{-1}), superior rate performance with a capacity retention of 57.8% when the current density increases 25 times from 0.2 to 5.0 C as well as a remarkable cycling performance with a capacity loss of 0.064% after 200 cycles at a high current density of 5.0 C.

EXPERIMENTAL

The ZnS NSs were fabricated through a hydrothermal method. Briefly, 0.446 g of $\text{Zn}(\text{NO}_3)_2 \cdot 6\text{H}_2\text{O}$ and 0.114 g of $\text{CS}(\text{NH}_2)_2$ were added into an aqueous solution containing 20 mL of diethylenetriamine (DETA) and 20 mL of deionized water

(DW) under magnetic stirring. Then, the mixed solution was transferred into a 50 mL Teflon-lined autoclave and placed in an oven at 180°C for 12 h. Afterward, the ZnS NSs were obtained by filtration with absolute alcohol and DW for several times. Then, 200 mg of ZnS NSs were dispersed in the 400 mL of DW under magnetic stirring followed by adding 484 mg of Tris-HCl buffer and 400 mg of dopamine (DA) to coat ZnS with polydopamine (PDA) *via* chemical polymerization for 1.0 h under stirring in air. After washing with DW and filtrating for several times, the dried products were further carbonized at 700°C for 2 h to produce ZnS@NC-NSs in N_2 . Then, the ZnS@NC-NSs were dispersed into aqueous ferric chloride (FeCl_3) solution and stirred over 12 h to convert the ZnS core into S because of the strong oxidizing ability of Fe^{3+} . Finally, the reactant was washed with 1 M HCl solution and DW to obtain S@NC-NSs after vacuum drying over night at 60°C.

Materials Characterizations

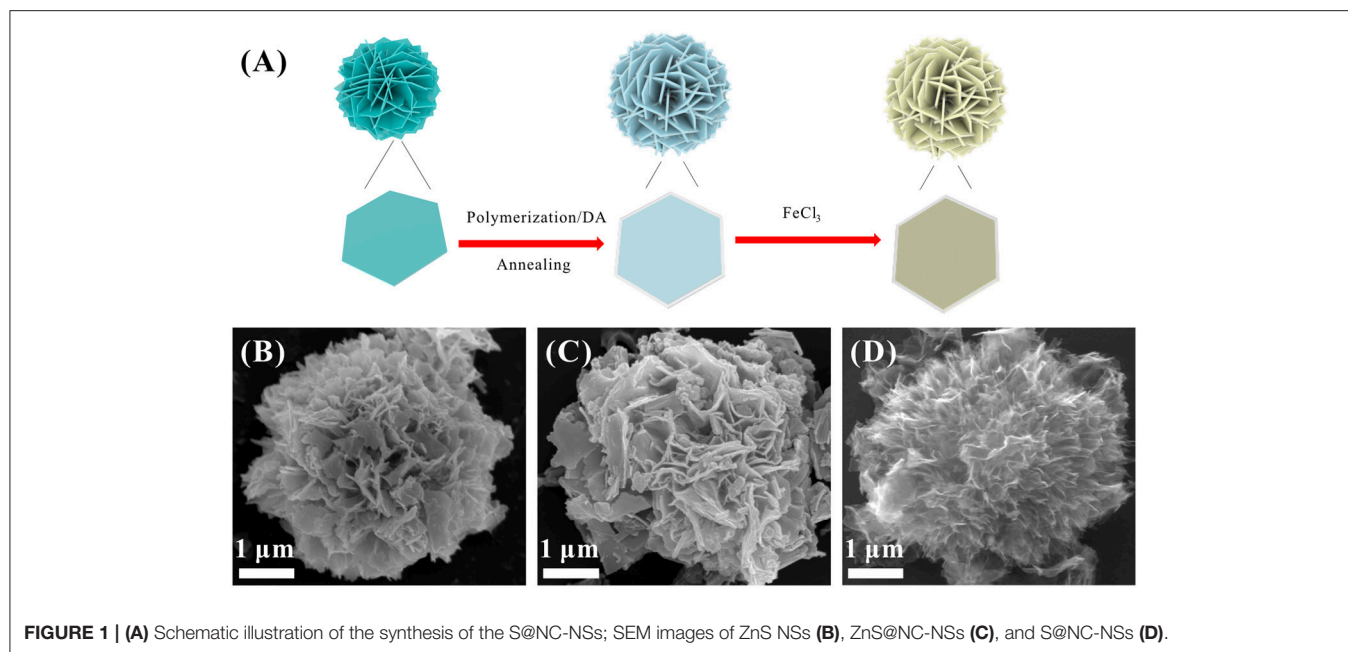
The morphology, structure and composition of ZnS NSs, ZnS@NC-NSs and S@NC-NSs were characterized by field-emission scanning electron microscopy (SEM, FEI Nova 450 Nano), transmission electron microscopy (TEM, JEM-2100 UHR STEM/EDS), X-ray photoelectron spectroscopy (ESCALAB 250Xi), and X-ray diffraction [XRD, Philips X'Pert Pro (Cu $\text{K}\alpha$ radiation, $\lambda = 1.5418 \text{ \AA}$)]. Micromeritics ASAP 2020 analyzer was applied to measure pore size distribution and the N_2 adsorption-desorption behavior of the NC shell. The S content in the S@NC-NSs was obtained by Naichi Corporation STA449C from room temperature to 600°C with a heating rate of 10°C min^{-1} in Ar. The concentration of LiPSs was determined by Ultraviolet-visible spectrophotometer (CARY 300).

Electrochemical Tests

The S@NC-NSs were mixed with acetylene black and polyvinylidene fluoride (PVDF) with a weight ratio of 7:2:1 to form a homogeneous slurry in N-Methyl-2-pyrrolidinone (NMP). Then, the slurry was uniformly coated on Al foil (15 μm) and vacuum dried at 60°C for 12 h. The coin-type cells were assembled with S@NC-NSs as cathode and Li metal foil as anode. The electrolyte consisted of 1 M lithium bis(trifluoromethane) sulfonimide (LiTFSI) in 1,3 dioxolane/1,2-dimethoxyethane (DOL/DME) (1:1, v/v) containing 0.2 M LiNO_3 . The electrochemical impedance spectroscopy (EIS) in the range of 100 kHz and 10 mHz and the cyclic voltammetry (CV) with a scan rate of 0.1 mV s^{-1} from 1.7 to 2.8 V were conducted on an electrochemical work station (CHI760E). The galvanostatic charging-discharging (GCD) tests were carried out on Neware battery testing system (CT-4008) with different current densities of 0.2, 0.5, 1.0, 1.5, 2.0, and 5.0 C.

RESULTS AND DISCUSSIONS

The synthesis procedure of S@NC-NSs is illustrated in **Figure 1A**. The ZnS NSs with a diameter of about 3–5 μm (**Figure 1B**), consisting of 2D nanosheets, were fabricated *via* a hydrothermal route. The XRD pattern of the as-obtained product (**Figure S1**) can be indexed into the wurtzite phase



ZnS (JCPDS Card No. 36-1450). The high resolution TEM (HR-TEM) image in **Figure S2A** indicates that the thickness of the ZnS NSs is 15–20 nm and discloses a lattice spacing of 0.31 nm corresponding to the (002) plane of wurtzite phase ZnS (Yao et al., 2005). Subsequently, a thin layer of amorphous C is uniformly coated on the surface of the ZnS NSs after the polymerization and annealing strategy. The ZnS@NC-NSs still maintain the flower-like morphology as can be seen from **Figure 1C**. During the chemical polymerization, PDA can adhere to the surface of the ZnS NSs, and further converted into the NC via annealing in N_2 . The HR-TEM image of the annealed product shows a typical core-shell structure with a crystal core and amorphous shell of 10–15 nm (**Figure S2B**). All XRD peaks of the carbon coated sample can also be assigned to the wurtzite phase ZnS (**Figure S3A**). And the XRD pattern (**Figure S3B**) and Raman spectra (**Figure S3C**) of the NC shell suggest that the obtained carbon shell is amorphous and has many defects. To further obtain the *in situ* formed S, the ZnS core of the ZnS@NC-NSs was oxidized to S by $FeCl_3$ solution according to the reaction of $ZnS (s) + 2Fe^{3+} (aq.) = Zn^{2+} (aq.) + S (s) + 2Fe^{2+} (aq.)$ (Ding et al., 2015; Ma et al., 2017). After oxidation, all diffraction patterns of the sample are corresponded to the orthorhombic S (JCPDS Card No. 08-0247) and no additional ZnS peaks can be observed (**Figure S4**). Meanwhile, the SEM image in **Figure 1D** indicates that S@NC-NSs can well preserve the morphology of flowers assembled by nanosheets, which is inherited from that of ZnS and ZnS@NC. Such a microflower structure is further confirmed in **Figure 2A**. The elemental mappings displayed in **Figure 2B** indicate that C, N, and S are uniformly distributed in the micro-sized flowers. The TEM image of the S@NC-NSs (**Figure 2C**) discloses that the nanosheets are hollow double-shell structures with a thickness of 25–40 nm, which provide enough void for the volume expansion

of sulfur upon the discharge process. EDS line scan of single S@NC-NSs demonstrates that S mainly exists in the inner wall of the hollow NC, which suggests that the *in situ* formed S is totally encapsulated and adhered to the inner surface of NC shell, as shown in **Figure 2D**. The mass loading of S in the S@NC-NSs can be optimized by varying the polymerization time. That is, the S@NC-NSs obtained at different polymerization time of 0.5, 1.0, and 2.0 h own different S mass loading of 65, 46.5 and 40.5% (**Figure S5A**), respectively. Among them, the sample polymerized 1.0 h shows the highest capacity and best cycling stability (**Figure S5B**), which is characterized in following study.

The X-ray photoelectron spectroscopy (XPS) is used to further analyze the chemical state of the S@NC-NSs. As shown in **Figure 3A**, the S@NC-NSs contain C, N, O, and S and no observable Zn signal is presented. The C 1s spectrum (**Figure 3B**) can be deconvoluted into three peaks centered at 284.6, 285.6, and 289.2 eV, corresponding to C–C/C=C (Li et al., 2016), C–S/C–N (Wang Z et al., 2014), and O–C=O (Yang et al., 2016), respectively. It is obvious that there are functional groups containing N/O in NC shell. The N 1s (**Figure 3C**) could be ascribed to three chemical states: pyridinic N (398.1 eV; Sun et al., 2012), pyrrolic N (400.1 eV; Peng et al., 2016), and quaternary N (400.8 eV; Cai et al., 2017), confirming the effective nitrogen doping of PDA derived carbon. The N doped carbon is beneficial for improving conductivity and wettability (Qiu et al., 2014; Chen et al., 2015). Moreover, in **Figure 3D**, 163.7 and 164.9 eV are corresponding to S–S/S–C bonds (Zhou et al., 2015b). These functional groups are reported to improve the chemical adsorption ability for LiPSs (See et al., 2014; Song et al., 2014; Chen et al., 2018).

In order to measure the pore structures of the NC shell, the S@NC-NSs were washed in CS_2 solution to remove the inner S and obtain the pure NC. The pore-sized distribution

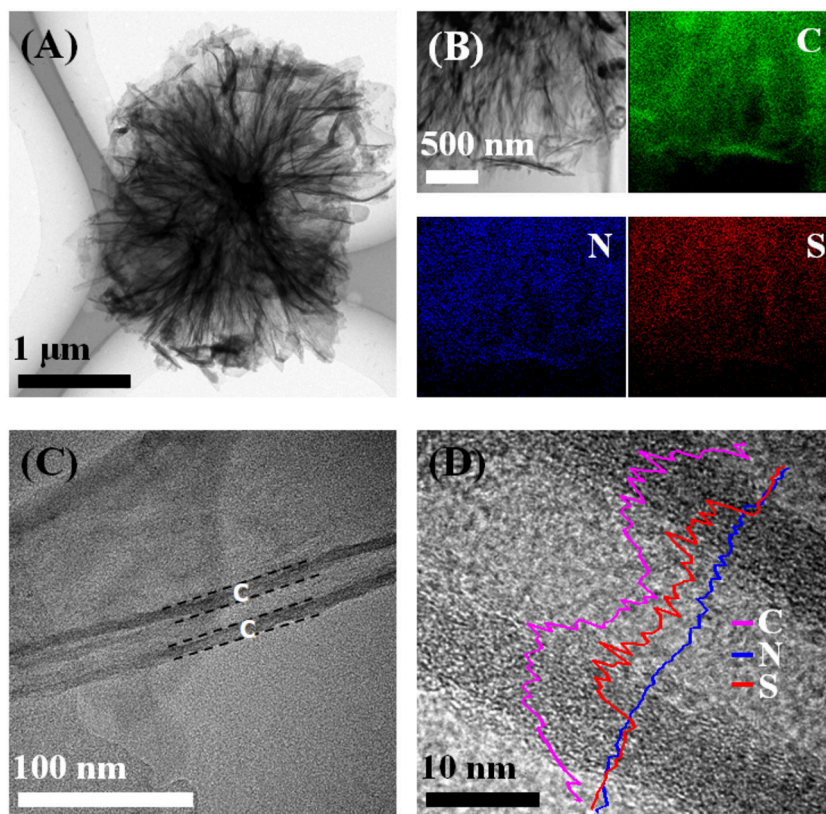


FIGURE 2 | The TEM image (A), elemental mappings (B), HRTEM image (C), and EDS line scan (D) of S@NC-NSs.

and the nitrogen adsorption-desorption isotherms of the pure NC are carried out and displayed in **Figure S6**. The NC shell with a BET surface area of $354.6 \text{ m}^2 \text{ g}^{-1}$ is mainly consisted of micropores, which is benefit for physically trapping LiPSs. To further evaluate the LiPSs trapping ability of the NC shell, the absorption experiment in orange Li_2S_6 solution was conducted. After adding 25 mg of NC shell into 5 mM Li_2S_6 solution (4 mL), the orange LiPSs solution turns colorless after 5.0 h (**Figure 4A**). Moreover, according to the UV-Vis spectra, the characteristic adsorption peaks at 310 ($\text{S}_6^{2-}/\text{S}_4^{2-}$) and 410 nm (S_4^{2-} ; (Xiao et al., 2015; Li X. et al., 2017)) have been eliminated after adding the NC shell (**Figure 4B**). Such results imply the strong adsorption capability of NC shell for LiPSs. This excellent adsorption performance is attributed to the physical trapping of the micropores below 2 nm (**Figure S6**) and chemical immobilization effect of the NC with fruitful O and N containing functional groups (Borchardt et al., 2016; Kang et al., 2016).

To illustrate the remarkable Li storage performance of S@NC-NSs, the coin cell type LSBs were fabricated. And the commercial S was used as the control sample. The cyclic voltammogram (CV) curves of S@NC-NSs and commercial S cathode between 1.7 and 2.8 V at a scan rate of 0.1 mV s^{-1} are presented in **Figure 5A**. In the cathodic process, the two reduction peaks between 1.98 and 2.30 V can be found in both samples, which

are assigned to the formation of soluble long-chain Li_2S_n ($4 \leq n \leq 8$) intermediates and solid lithium sulfide (Li_2S_2 or Li_2S). In the subsequent anodic process, the CV curve of S@NC-NSs shows two individual peaks at 2.37 and 2.43 V on virtue of the reactions from lithium sulfide to Li_2S_n ($4 \leq n \leq 8$) and S, while the commercial S only shows a broaden peak at 2.42 V because of the large polarization. Compared to the commercial S electrode, it is clearly seen that the oxidation and reduction peaks of the S@NC-NSs electrode are sharper and shift toward the quasi-equilibrium potential, revealing lower polarization and higher reaction kinetics. **Figure 5B** presents charge-discharge curves of the S@NC-NSs electrode at 0.2, 0.5, 1.0, 1.5, 2.0, and 5.0 C. Two typical plateaus of the S@NC-NSs cathode can be observed at 0.2 C in discharge process delivering a high capacity of $1,238 \text{ mAh g}^{-1}$. Even at a high current density of 5.0 C, a remarkable plateau at 1.9 V still exists due to the rapid kinetics of the S@NC-NSs electrode. The capacity retention of the S@NC-NSs cathode is 57.8% when the current density increases 25 times from 0.2 to 5.0 C, which is much better than that of the commercial S electrode, as shown in **Figure 5C**. The capacity and rate performance of S@NC-NSs are competitive among recently reported S/C composite electrodes (Xia et al., 2017; Zhu et al., 2017; Wang X et al., 2018; Yao et al., 2018). Furthermore, once the rate is reverted back to 0.5 C, the specific capacity of 920 mAh g^{-1} is obtained, revealing its excellent reversibility and

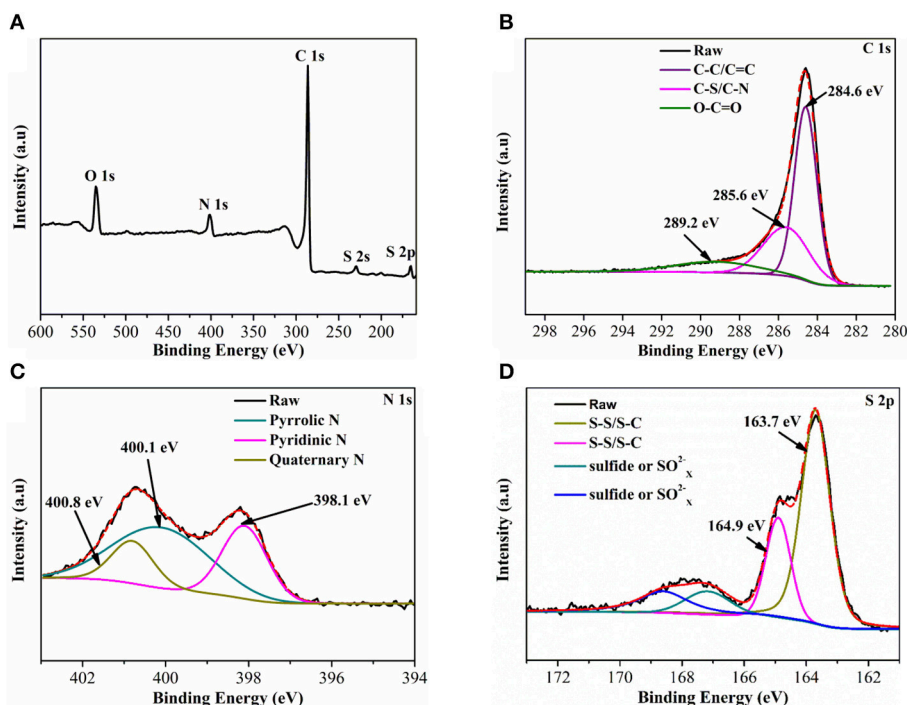


FIGURE 3 | (A) Full XPS spectrum of S@NC-NSs; **(B–D)** High-resolution spectrum of C1s, N 1s, and S 2p, respectively.

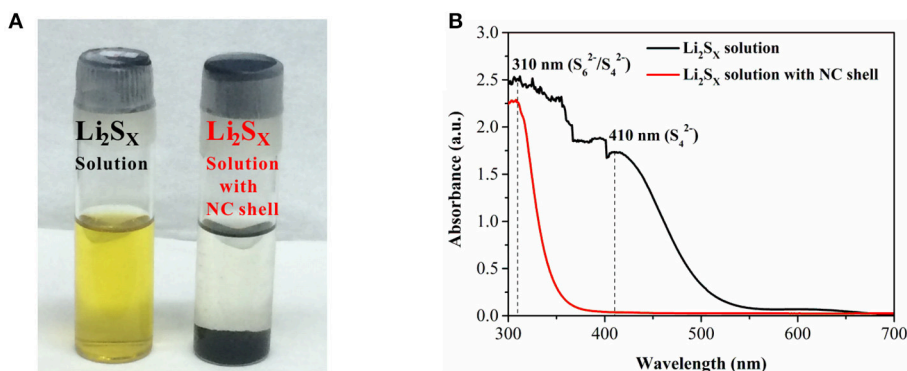


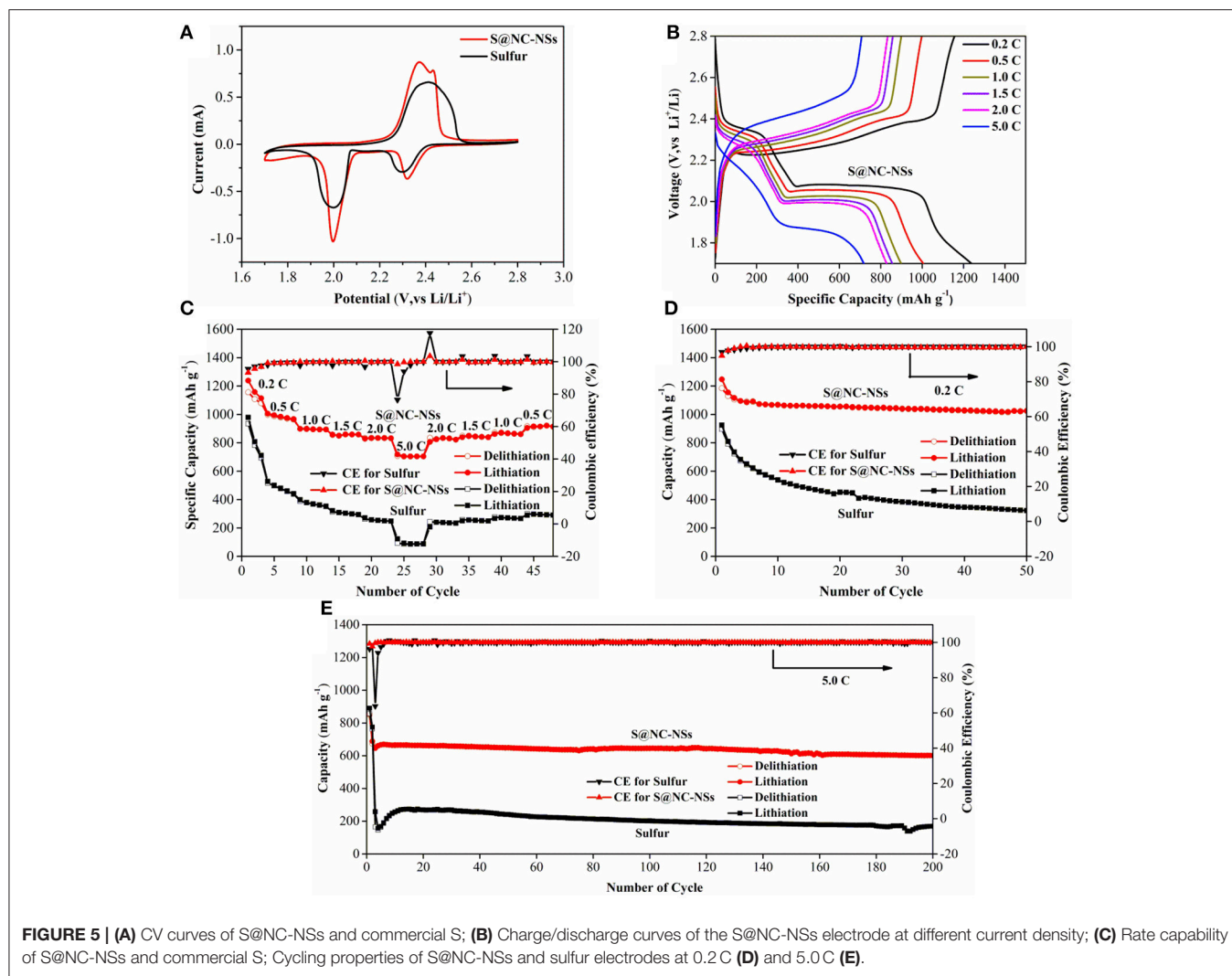
FIGURE 4 | (A) Adsorption properties of NC shell in Li_2S_6 solution; **(B)** UV-Vis absorption spectra after adding NC shell.

rate performance. **Figure 5D** displays the cyclability of S@NC-NSs and commercial sulfur cathodes at the current density of 0.2 C. Although the S@NC-NSs cathode has an obvious capacity decay at first three cycles, afterwards, it delivers a high and stable capacity of $1,025 \text{ mAh g}^{-1}$ over 50 cycles, which is far exceeding that of pure S. Even at a high current density of 5.0 C (**Figure 5E**), the S@NC-NSs cathode achieves a high capacity of 600 mAh g^{-1} over 200 cycles with a low decay rate of 0.064%. Furthermore, the Nyquist plots of commercial S and S@NC-NSs cathodes after 200 cycles at 5.0 C between 100 kHz and 0.01 Hz are shown in **Figure S7**. The equivalent impedance of the S@NC-NSs cathode is much smaller than the commercial S cathode, indicating a faster electrons/ions transportation because

of special structures of S@NC-NSs assembled by micro-sized flowers with high conductivity. The outstanding cycling stability of S@NC-NSs cathodes can be attributed to dual functions of NC shell with both physical trapping and chemical immobilization of LiPSs.

CONCLUSION

In summary, a dual-shell and hollow S@NC-NSs assembled by micro-sized flowers are fabricated for LSBs *via in situ* oxidation process. The *in situ* generated S is encapsulated and adheres to the inner wall of the NC shell with abundant micropores and fruitful N or O containing function groups,



which offers both physical trapping and chemical tethering to eliminate the shuttle effect of LiPSs. Moreover, the conjoint hollow NC-NSs also provide high conductive channels for electron transport and enough space for volumetric expansion of S. The S mass loading of S@NC-NSs can be easily adjusted *via* tuning the thickness of the carbon shell. As the Li-S battery cathode, the S@NC-NSs achieve a high capacity of $1,238 \text{ mAh g}^{-1}$ at 0.2 C and outstanding rate performance with capacity retention of the 57.8% when the current density increased 25 times from 0.2 to 5.0 C. Importantly, S@NC-NSs demonstrate the excellent stability with a high capacity of 600 mAh g^{-1} and an ultraslow capacity decay rate of 0.064% after 200 cycles at a high current density of 5.0 C. With high conductivity, efficient physical and chemical immobilization as well as adequate inner space, the NC encapsulated *in situ* formed S cathode with outstanding electrochemical performance can bode well for promising application in LSBs.

AUTHOR CONTRIBUTIONS

ZG carried out the experiment and wrote the paper. BG and XF supervised this research. XL, HS, KD, and XH gave a lot of help for analyzing data. XZ, XP and JF helped writing.

ACKNOWLEDGMENTS

This work was financially supported by National Natural Science Foundation of China (No. 51572100 and 51504171) and Major project of Technology Innovation of Hubei Province (2018AAA011).

SUPPLEMENTARY MATERIAL

The Supplementary Material for this article can be found online at: <https://www.frontiersin.org/articles/10.3389/fchem.2018.00429/full#supplementary-material>

REFERENCES

- Borchardt, L., Oschatz, M., and Kaskel, S. (2016). Carbon materials for lithium sulfur batteries—ten critical questions. *Chem. Eur. J.* 22, 7324–7351. doi: 10.1002/chem.201600040
- Cai, Q., Li, Y., Wang, L., Li, Q., Xu, J., Gao, B., et al. (2017). Freestanding hollow double-shell Se@CNx nanobelts as large-capacity and high-rate cathodes for Li-Se batteries. *Nano Energy* 32, 1–9. doi: 10.1016/j.nanoen.2016.12.010
- Chabu, J. M., Zeng, K., Walle, M. D., You, X., Zhang, M., Li, Y., et al. (2017). Facile fabrication of sulfur/graphene composite for high-rate lithium-sulfur batteries. *ChemistrySelect* 2, 11035–11039. doi: 10.1002/slct.201702336
- Chen, J., Yuan, R., Feng, J., Zhang, Q., Huang, J., Fu, G., et al. (2015). Conductive Lewis base matrix to recover the missing link of Li₂S₈ during the sulfur redox cycle in Li-S battery. *Chem. Mater.* 27, 2048–2055. doi: 10.1021/cm5044667
- Chen, K., Sun, Z., Fang, R., Shi, Y., Cheng, H. M., and Li, F. (2018). Metal-organic frameworks (MOFs)-derived nitrogen-doped porous carbon anchored on graphene with multifunctional effects for lithium-sulfur batteries. *Adv. Funct. Mater.* 1707592. doi: 10.1002/adfm.201707592
- Chen, T., Zhang, Z., Cheng, B., Chen, R., Hu, Y., Ma, L., et al. (2017). Self-templated formation of interlaced carbon nanotubes threaded hollow Co₃S₄ nanoboxes for high-rate and heat-resistant lithium-sulfur batteries. *J. Am. Chem. Soc.* 139, 12710–12715. doi: 10.1021/jacs.7b06973
- Ding, N., Lum, Y., Chen, S., Chien, S. W., Hor, T. A., Liu, Z., et al. (2015). Sulfur-carbon yolk-shell particle based 3D interconnected nanostructures as cathodes for rechargeable lithium-sulfur batteries. *J. Mater. Chem. A* 3, 1853–1857. doi: 10.1039/C4TA05659K
- Du, Z., Guo, C., Wang, L., Hu, A., Jin, S., Zhang, T., et al. (2017). Atom-thick interlayer made of cvd-grown graphene film on separator for advanced lithium-sulfur batteries. *ACS Appl. Mater. Interfaces* 9, 43696–43703. doi: 10.1021/acsami.7b14195
- Kang, W., Deng, N., Ju, J., Li, Q., Wu, D., Ma, X., et al. (2016). A review of recent developments in rechargeable lithium-sulfur batteries. *Nanoscale* 8, 16541–16588. doi: 10.1039/C6NR04923K
- Li, C., Xi, Z., Guo, D., Chen, X., and Yin, L. (2018). Chemical immobilization effect on lithium polysulfides for lithium-sulfur batteries. *Small* 14:1701986. doi: 10.1002/smll.201701986
- Li, F., Qin, F., Zhang, K., Fang, J., Lai, Y., and Li, J. (2017). Hierarchically porous carbon derived from banana peel for lithium sulfur battery with high areal and gravimetric sulfur loading. *J. Power Sources* 362, 160–167. doi: 10.1016/j.jpowsour.2017.07.038
- Li, M., Carter, R., Douglas, A., Oakes, L., and Pint, C. L. (2017). Sulfur vapor-infiltrated 3D carbon nanotube foam for binder-free high areal capacity lithium-sulfur battery composite cathodes. *ACS Nano* 11, 4877–4884. doi: 10.1021/acsnano.7b01437
- Li, X., Ding, K., Gao, B., Li, Q., Li, Y., Fu, J., et al. (2017). Freestanding carbon encapsulated mesoporous vanadium nitride nanowires enable highly stable sulfur cathodes for lithium-sulfur batteries. *Nano Energy* 40, 655–662. doi: 10.1016/j.nanoen.2017.09.018
- Li, Y., Cai, Q., Wang, L., Li, Q., Peng, X., Gao, B., et al. (2016). Mesoporous TiO₂ nanocrystals/graphene as an efficient sulfur host material for high-performance lithium-sulfur batteries. *ACS Appl. Mater. Interfaces* 8, 23784–23792. doi: 10.1021/acsami.6b09479
- Liu, Z., Liu, B., Guo, P., Shang, X., Lv, M., Liu, D., et al. (2018). Enhanced electrochemical kinetics in lithium-sulfur batteries by using carbon nanofibers/manganese dioxide composite as a bifunctional coating on sulfur cathode. *Electrochim. Acta* 269, 180–187. doi: 10.1016/j.electacta.2018.02.160
- Ma, T., Zhou, F., Zhang, T. W., Yao, H. B., Su, T. Y., Yu, Z. L., et al. (2017). Large-scale syntheses of zinc sulfide-(diethylenetriamine)_{0.5} hybrids as precursors for sulfur nanocomposite cathodes. *Angew. Chem. Int. Ed.* 56, 11836–11840. doi: 10.1002/anie.201706199
- Moreno, N., Agostini, M., Caballero, A., Morales, J., and Hassoun, J. (2015). A long-life lithium ion sulfur battery exploiting high performance electrodes. *Chem. Commun.* 51, 14540–14542. doi: 10.1039/C5CC05162B
- Pang, Q., Tang, J., Huang, H., Liang, X., Hart, C., Tam, K. C., et al. (2015). A Nitrogen and sulfur dual-doped carbon derived from polyrhodanine@cellulose for advanced lithium-sulfur batteries. *Adv. Mater.* 27, 6021–6028. doi: 10.1002/adma.201502467
- Peng, H. J., Zhang, Z. W., Huang, J. Q., Zhang, G., Xie, J., Xu, W. T., et al. (2016). A cooperative interface for highly efficient lithium-sulfur batteries. *Adv. Mater.* 28, 9551–9558. doi: 10.1002/adma.201603401
- Qiu, Y., Li, W., Zhao, W., Li, G., Hou, Y., Liu, M., et al. (2014). High-rate, ultralong cycle-life lithium/sulfur batteries enabled by nitrogen-doped graphene. *Nano Lett.* 14, 4821–4827. doi: 10.1021/nl5020475
- Qu, H., Zhang, J., Du, A., Chen, B., Chai, J., Xue, N., et al. (2018). Multifunctional sandwich-structured electrolyte for high-performance lithium-sulfur batteries. *Adv. Sci.* 5:1700503. doi: 10.1002/advs.201700503
- Qu, Y., Zhang, Z., Wang, X., Lai, Y., Liu, Y., and Li, J. (2013). A simple SDS-assisted self-assembly method for the synthesis of hollow carbon nanospheres to encapsulate sulfur for advanced lithium-sulfur batteries. *J. Mater. Chem. A* 1, 14306–14310. doi: 10.1039/c3ta13306k
- Rehman, S., Guo, S., and Hou, Y. (2016). Rational design of Si/SiO₂@hierarchical porous carbon spheres as efficient polysulfide reservoirs for high-performance Li-S battery. *Adv. Mater.* 28, 3167–3172. doi: 10.1002/adma.201506111
- See, K. A., Jun, Y. S., Gerbec, J. A., Sprafke, J. K., Wudl, F., Stucky, G. D., et al. (2014). Sulfur-functionalized mesoporous carbons as sulfur hosts in Li-S batteries: increasing the affinity of polysulfide intermediates to enhance performance. *ACS Appl. Mater. Interfaces* 6, 10908–10916. doi: 10.1021/am405025n
- Seh, Z. W., Sun, Y., Zhang, Q., and Cui, Y. (2016). Designing high-energy lithium-sulfur batteries. *Chem. Soc. Rev.* 45, 5605–5634. doi: 10.1039/C5CS00410A
- Shi, H., Lv, W., Zhang, C., Wang, D., Ling, G., He, Y., et al. (2018). Functional carbons remedy the shuttling of polysulfides in lithium-sulfur batteries: confining, trapping, blocking, and breaking up. *Adv. Funct. Mater.* 1800508. doi: 10.1002/adfm.201800508
- Song, J., Xu, T., Gordin, M. L., Zhu, P., Lv, D., Jiang, Y. B., et al. (2014). Nitrogen-doped mesoporous carbon promoted chemical adsorption of sulfur and fabrication of high-areal-capacity sulfur cathode with exceptional cycling stability for lithium-sulfur batteries. *Adv. Funct. Mater.* 24, 1243–1250. doi: 10.1002/adfm.201302631
- Song, Y., Zhao, W., Zhu, X., Zhang, L., Li, Q., Ding, F., et al. (2018). Vanadium dioxide-graphene composite with ultrafast anchoring behavior of polysulfides for lithium-sulfur batteries. *ACS Appl. Mater. Interfac.* 10, 15733–15741. doi: 10.1021/acsami.8b02920
- Sun, F., Tang, H., Zhang, B., Li, X., Yin, C., Yue, Z., et al. (2018). PEO-linked MoS₂-graphene nanocomposites with 2D polar-nonpolar amphoteric surfaces as sulfur hosts for high-performance Li-S batteries. *ACS Sustain. Chem. Eng.* 6, 974–982. doi: 10.1021/acssuschemeng.7b03306
- Sun, L., Wang, L., Tian, C., Tan, T., Xie, Y., Shi, K., et al. (2012). Nitrogen-doped graphene with high nitrogen level via a one-step hydrothermal reaction of graphene oxide with urea for superior capacitive energy storage. *RSC Adv.* 2, 4498–4506. doi: 10.1039/c2ra01367c
- Tang, C., Li, B., Zhang, Q., Zhu, L., Wang, H., Shi, J., et al. (2016). CaO-templated growth of hierarchical porous graphene for high-power lithium-sulfur battery applications. *Adv. Funct. Mater.* 26, 577–585. doi: 10.1002/adfm.201503726
- Wang, Q., Wang, Z., Li, R., Liu, H., Yang, M., Li, C., et al. (2018). Flower-like nitrogen-oxygen-doped carbon encapsulating sulfur composite synthesized via in-situ oxidation approach. *Chem. Eng. J.* 345, 271–279. doi: 10.1016/j.cej.2018.03.179
- Wang, X., Bi, X., Wang, S., Zhang, Y., Du, H., and Lu, J. (2018). High-rate and long-term cycle stability of Li-S batteries enabled by Li₂S/TiO₂-impregnated hollow carbon nanofiber cathodes. *ACS Appl. Mater. Interfaces* 10, 16552–16560. doi: 10.1021/acsami.8b03201
- Wang, X., Gao, T., Han, F., Ma, Z., Zhang, Z., Li, J., et al. (2016). Stabilizing high sulfur loading Li-S batteries by chemisorption of polysulfide on three-dimensional current collector. *Nano Energy* 30, 700–708. doi: 10.1016/j.nanoen.2016.10.049
- Wang, X., Yang, C., Xiong, X., Chen, G., Huang, M., Wang, J. H., et al. (2019). A robust sulfur host with dual lithium polysulfide immobilization mechanism for long cycle life and high capacity Li-S batteries. *Energy Storage Mater.* 16, 344–353. doi: 10.1016/j.ensm.2018.06.015
- Wang, X., Zhang, Z., Qu, Y., Lai, Y., and Li, J. (2014). Nitrogen-doped graphene/sulfur composite as cathode material for high capacity lithium-sulfur batteries. *J. Power Sources* 256, 361–368. doi: 10.1016/j.jpowsour.2014.01.093
- Wang, Z., Dong, Y., Li, H., Zhao, Z., Wu, H. B., Hao, C., et al. (2014). Enhancing lithium-sulphur battery performance by strongly binding the

- discharge products on amino-functionalized reduced graphene oxide. *Nat. Commun.* 5:5002. doi: 10.1038/ncomms6002
- Xia, Y., Fang, R., Xiao, Z., Huang, H., Gan, Y., Yan, R., et al. (2017). Confining sulfur in N-doped porous carbon microspheres derived from microalgae for advanced lithium-sulfur batteries. *ACS Appl. Mater. Interfaces* 9, 23782–23791. doi: 10.1021/acsami.7b05798
- Xiao, Z., Yang, Z., Wang, L., Nie, H., Zhong, M., Lai, Q., et al. (2015). A lightweight TiO₂/graphene interlayer, applied as a highly effective polysulfide adsorbent for fast, long-life lithium-sulfur batteries. *Adv. Mater.* 27, 2891–2898. doi: 10.1002/adma.201405637
- Xu, G., Kushima, A., Yuan, J., Dou, H., Xue, W., Zhang, X., et al. (2017). *Ad hoc* solid electrolyte on acidized carbon nanotube paper improves cycle life of lithium-sulfur batteries. *Energy Environ. Sci.* 10, 2544–2551. doi: 10.1039/C7EE01898C
- Yang, J., Chen, F., Li, C., Bai, T., Long, B., and Zhou, X. (2016). A free-standing sulfur-doped microporous carbon interlayer derived from luffa sponge for high performance lithium-sulfur batteries. *J. Mater. Chem. A* 4, 14324–14333. doi: 10.1039/C6TA06250D
- Yao, W. T., Yu, S. H., Pan, L., Li, J., Wu, Q. S., Zhang, L., et al. (2005). Flexible wurtzite-type ZnS nanobelts with quantum-size effects: a diethylenetriamine-assisted solvothermal approach. *Small* 1, 320–325. doi: 10.1002/smll.200400079
- Yao, X., Xu, J., Hong, Z., Li, G., Wang, X., Lu, F., et al. (2018). Metal/graphene composites with strong metal-S bondings for sulfur immobilization in Li-S batteries. *J. Phys. Chem. C* 122, 3263–3272. doi: 10.1021/acs.jpcc.7b12063
- Ye, Y., Wu, F., Xu, S., Qu, W., Li, L., and Chen, R. (2018). Designing realizable and scalable techniques for practical lithium sulfur batteries: a perspective. *J. Phys. Chem. Lett.* 9, 1398–1414. doi: 10.1021/acs.jpcclett.7b03165
- Zhang, Q., Chen, H., Luo, L., Zhao, B., Luo, H., and Han, X. (2018). Harnessing the concurrent reaction dynamics in active Si and Ge to achieve high performance lithium-ion batteries. *Energy Environ. Sci.* 11, 669–681. doi: 10.1039/C8EE00239H
- Zhou, G., Paek, E., Hwang, G. S., and Manthiram, A. (2015a). Long-life Li/polysulfide batteries with high sulphur loading enabled by lightweight three-dimensional nitrogen/sulphur-codoped graphene sponge. *Nat. Commun.* 6:7760. doi: 10.1038/ncomms8760
- Zhou, G., Zhao, Y., and Manthiram, A. (2015b). Dual-confined flexible sulfur cathodes encapsulated in nitrogen-doped double-shelled hollow carbon spheres and wrapped with graphene for Li-S batteries. *Adv. Energy Mater.* 5:1402263. doi: 10.1002/aenm.2014.02263
- Zhou, H., Wang, D., Fu, A., Liu, X., Wang, Y., Li, Y., et al. (2017). Mesoporous carbon spheres with tunable porosity prepared by a template-free method for advanced lithium-sulfur batteries. *Mater. Sci. Eng. B* 227, 9–15. doi: 10.1016/j.mseb.2017.10.005
- Zhu, Q., Zhao, Q., An, Y., Anasori, B., Wang, H., and Xu, B. (2017). Ultra-microporous carbons encapsulate small sulfur molecules for high performance lithium-sulfur battery. *Nano Energy* 33, 402–409. doi: 10.1016/j.nanoen.2017.01.060

Conflict of Interest Statement: The authors declare that the research was conducted in the absence of any commercial or financial relationships that could be construed as a potential conflict of interest.

Copyright © 2018 Guo, Feng, Li, Zhang, Peng, Song, Fu, Ding, Huang and Gao. This is an open-access article distributed under the terms of the Creative Commons Attribution License (CC BY). The use, distribution or reproduction in other forums is permitted, provided the original author(s) and the copyright owner(s) are credited and that the original publication in this journal is cited, in accordance with accepted academic practice. No use, distribution or reproduction is permitted which does not comply with these terms.